



# A viable dipole magnet concept with REBCO CORC<sup>®</sup> wires and further development needs for high-field magnet applications

Xiaorong Wang<sup>1</sup> , Shlomo Caspi<sup>1</sup>, Daniel R Dietderich<sup>1</sup>, William B Ghiorso<sup>1</sup>, Stephen A Gourlay<sup>1</sup>, Hugh C Higley<sup>1</sup>, Andy Lin<sup>1</sup>, Soren O Prestemon<sup>1</sup>, Danko van der Laan<sup>2,3</sup>  and Jeremy D Weiss<sup>2,3</sup>

<sup>1</sup> Lawrence Berkeley National Laboratory, Berkeley, CA 94720, United States of America

<sup>2</sup> Advanced Conductor Technologies, Boulder, CO 80301, United States of America

<sup>3</sup> University of Colorado, Boulder, CO 80301, United States of America

E-mail: [xrwang@lbl.gov](mailto:xrwang@lbl.gov)

Received 27 December 2017, revised 1 February 2018

Accepted for publication 7 February 2018

Published 6 March 2018



## Abstract

REBCO coated conductors maintain a high engineering current density above 16 T at 4.2 K. That fact will significantly impact markets of various magnet applications including high-field magnets for high-energy physics and fusion reactors. One of the main challenges for the high-field accelerator magnet is the use of multi-tape REBCO cables with high engineering current density in magnet development. Several approaches developing high-field accelerator magnets using REBCO cables are demonstrated. In this paper, we introduce an alternative concept based on the canted  $\cos \theta$  (CCT) magnet design using conductor on round core (CORC<sup>®</sup>) wires that are wound from multiple REBCO tapes with a Cu core. We report the development and test of double-layer three-turn CCT dipole magnets using CORC<sup>®</sup> wires at 77 and 4.2 K. The scalability of the CCT design allowed us to effectively develop and demonstrate important magnet technology features such as coil design, winding, joints and testing with minimum conductor lengths. The test results showed that the CCT dipole magnet using CORC<sup>®</sup> wires was a viable option in developing a REBCO accelerator magnet. One of the critical development needs is to increase the engineering current density of the 3.7 mm diameter CORC<sup>®</sup> wire to 540 A mm<sup>-2</sup> at 21 T, 4.2 K and to reduce the bending radius to 15 mm. This would enable a compact REBCO dipole insert magnet to generate a 5 T field in a background field of 16 T at 4.2 K.

Keywords: REBCO, dipole magnet, CORC<sup>®</sup>

(Some figures may appear in colour only in the online journal)

## 1. Introduction

Future high-energy proton–proton colliders will require dipole magnetic fields of the order of 16 T or greater [1, 2]. Dipole magnets that generate such high fields will need superconductors that can carry a high current at 16 T and 4.2 K. REBa<sub>2</sub>Cu<sub>3</sub>O<sub>x</sub> (REBCO, RE = rare earth) coated conductor technology is a strong candidate that can meet this requirement. More than ten vendors worldwide are developing commercial conductors that can potentially lower the

conductor cost and benefit high-field REBCO magnet applications for high-energy physics and compact fusion reactors [3].

Compared to the significant progress in high-field solenoid magnets made with REBCO tapes [4–9], the development of REBCO high-field accelerator magnets is less advanced, limited by the use of single tapes [10–14]. Two technical issues can partially explain this. First, the flat thin tape geometry makes it difficult to develop multi-strand high-current cables, which are the *de facto* conductor form for

high-field accelerator magnets [15]. Cables enable high currents and lower magnet inductance, which is motivated by quench protection issues. Second, performance of accelerator magnets based on the few REBCO cable architectures available is still largely unknown.

To address these two challenging and intertwined issues, the European EuCARD-2 collaboration [16, 17] has been developing REBCO Roebel cables [18] and the associated dipole magnet demonstration based on the aligned block [19] and  $\cos \theta$  designs [20]. Recently, the CERN group successfully tested an aligned-block dipole magnet that reached 3 T in 5 K helium gas [21]. A dipole design using twisted stacked tape cables [22] is also under investigation [23].

Complementary to these studies, we present an alternative concept for future high-field REBCO accelerator insert magnets. It is based on the canted  $\cos \theta$  (CCT) design using REBCO conductor on round core (CORC<sup>®</sup>) wires. The CORC<sup>®</sup> wires are developed at Advanced Conductor Technologies, LLC (ACT) by winding multiple layers of REBCO tapes in a helical fashion around a Cu former [24–26]. Compared to Roebel cables, CORC<sup>®</sup> wires are isotropic in terms of bending and electromagnetic behavior which can potentially simplify magnet design and fabrication. The partially transposed multi-tape configuration can reduce AC losses [27] and allow current sharing inside CORC<sup>®</sup> wires, a desirable feature for magnet quench protection. Compared to the same amount of REBCO tapes assembled in a stack or Roebel cable, the Cu former reduces the engineering current density ( $J_e$ ) of the CORC<sup>®</sup> wires which is defined as the current per unit cross sectional area of the wire. On the other hand, the Cu former can allow thinner Cu plating of REBCO tapes to maintain the same copper fraction as some other REBCO cable concepts.

The CCT magnet design was introduced by Meyer and Flasck in 1970 [28]. It promises several features attractive for high-field accelerator magnet applications, including effective stress management, simple magnet fabrication and excellent geometric field quality [29–33]. Lawrence Berkeley National Laboratory has been developing CCT magnet technology for high-field accelerator magnets using both low- and high-temperature superconductors [34, 35].

Because of these unique features of CORC<sup>®</sup> wires and CCT magnet design, we expect the CORC<sup>®</sup> CCT concept to be a viable option for future high-field REBCO accelerator insert magnets. Here, we report the proof-of-principle development of two double-layer three-turn CCT dipole magnets using the CORC<sup>®</sup> wires as an essential step to demonstrate the viability of the concept. The tests showed that the concept is feasible and we foresee no fundamental technical issues to develop magnets with additional turns and higher fields. In section 2, we review the main parameters of the CORC<sup>®</sup> wires used here, followed by the details of design, fabrication and testing of CCT dipole magnets in sections 3 and 4. We present the main test results at 77 and 4.2 K in section 5. In section 6, we discuss the implications and several aspects on both conductor and magnet technology that will benefit from further development.



**Figure 1.** The commercial CORC<sup>®</sup> wire manufactured by Advanced Conductor Technologies, LLC. A polyester heat shrink tube encapsulates multiple layers of REBCO tapes helically wound on a Cu core.

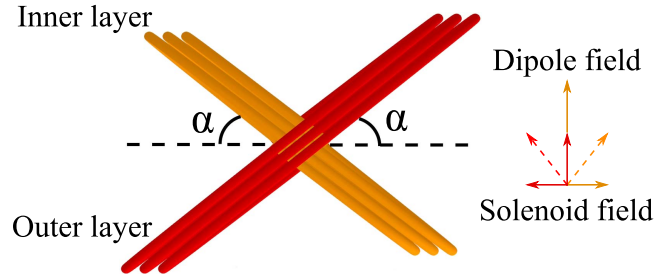


**Figure 2.** Illustration of the two-layer three-turn CCT dipole magnet using CORC<sup>®</sup> wires. The field from each layer cancels the solenoid component and doubles the dipole components in the aperture.

**Table 1.** Parameters of the two types of CORC<sup>®</sup> wires used for the three-turn CCT magnets C0a and C0b.

		16-tape wire	29-tape wire
Magnet name	—	C0a	C0b
Wire diameter	mm	3.09	3.63
Diameter of Cu core	mm	2.34	2.56
Number of tapes	—	16	29
Tape width	mm	2	2
Cu plating thickness	$\mu\text{m}$	5	5
Substrate thickness	$\mu\text{m}$	30	30
Cross sectional area	$\text{mm}^2$	7.5	10.35
Percentage of Cu area	—	62%	55%
Wire length	m	2.3	2.9

## 2. CORC<sup>®</sup> wire layout

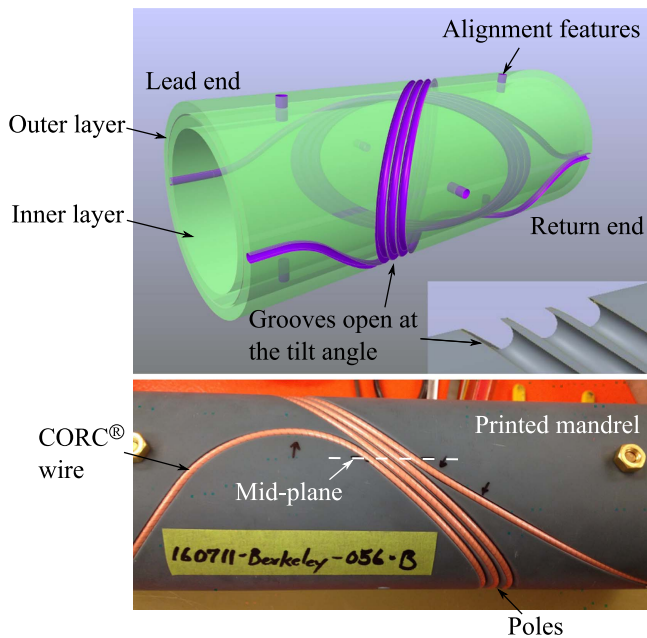
Figure 1 shows a segment of the CORC<sup>®</sup> wire developed by ACT. Two CORC<sup>®</sup> wire designs were used to make the CCT magnets. The first design contained 16 tapes whereas the second one contained 29 tapes. The commercial REBCO tapes (SCS-2030) were manufactured by SuperPower Incorporated (SPI). They were 2 mm wide, 45  $\mu\text{m}$  thick, and contained a 30  $\mu\text{m}$  thick substrate. Table 1 compares the main parameters of both wires.

## 3. Magnet design and fabrication

The CCT test magnets consisted of two layers with three turns of CORC<sup>®</sup> wire in each layer (figure 2). With respect to the bore axial direction, the wires tilted at an angle ( $\alpha$ ) to cancel

**Table 2.** Design parameters for the three-turn CCT dipole magnets C0a and C0b.

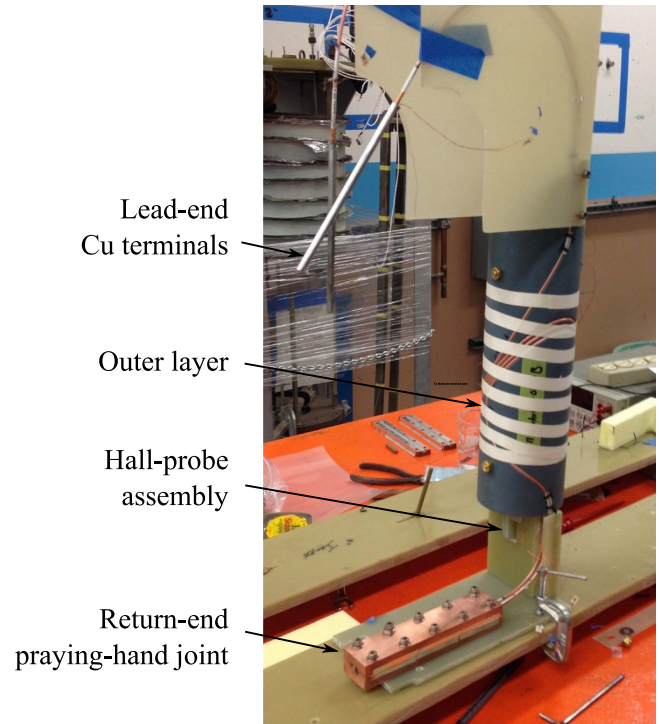
		C0a	C0b
Inner diameter	mm	70	85
Outer diameter	mm	94	111.4
Turn	—	3	3
Layer	—	2	2
Tilt angle	degree	40	40
Minimum bending radius at magnet pole	mm	25	30.1
Radial gap between layers	mm	1	1
Groove diameter	mm	3.5	4.1
Mandrel thickness	mm	5.5	6.1
Rib thickness at the mid-plane	mm	0.5	0.5
Wire pitch length over one turn	mm	6.22	7.16
Mandrel length	mm	300	275

**Figure 3.** Top: a 3D model of the assembled C0a magnet. The inset gives a close-up of the ‘U’-shaped grooves. Bottom: the outer layer of C0a. The white dashed line illustrates the mid-plane of the magnets. The bottom pole region is also shown.

the solenoid field components produced by each layer and double the dipole field in the magnet aperture [32, 33].

Magnet C0a had an aperture of 70 mm in order to measure the field quality of a longer version of C0a using the existing measurement hardware. Given the magnet aperture and allowable wire bending radius, we chose a tilt angle of 40° for C0a with the 16-tape wire. Magnet C0b had the same tilt angle but a larger aperture of 85 mm to increase the bending radius of the 29-tape wire. Table 2 gives the main design parameters for both magnets. Here the bending radius is determined along the wire longitudinal axis. The rib thickness refers to the minimum distance between the two neighboring wires at the magnet mid-plane (figure 3).

The tilted turns in figure 2 were located in the ‘U’-shaped grooves in the mandrels. The grooves were parallel at an

**Figure 4.** Assembled C0a magnet before the cold test.

angle rather than being normal to the mandrel surface (figure 3). This feature allowed us to wind the CCT magnet as if it were a solenoid, including applying tension, if needed, to the conductor during winding.

In addition to the tilted conductor turns, lead wires were arranged to facilitate the fabrication of electrical joints. The bending radii of the lead wires were larger than the minimum bending radius at the magnet poles to reduce the wire bend. At the lead end, the wires from each layer exited the mandrel 180° apart (figure 3). At the return end, the conductors exited the mandrel at the same angular position. This configuration minimized the wire bend when making the return-end joints.

The mandrel was printed using Accura® Bluestone®, a composite material for manufacturing stable and high stiffness parts [36]. The material can be used in liquid nitrogen and liquid helium. At 77 K, it has an ultimate tensile strength of 190 MPa and an ultimate flexural strength of 105 MPa [37]. Therefore, the mandrel was strong enough for the self-field test of the three-turn magnets. The Bluestone® contracts about 0.65% from room temperature to 4.2 K [37], about twice that of Cu. Note that Cu dominated the CORC® wire in terms of volume. The over-sized groove diameter can compensate the larger shrinkage of the mandrel with respect to the conductor.

Although the groove design allowed winding with tension on wires, both proof-of-principle magnets were hand-wound with no tension on the wire to minimize the wire handling. After winding each layer, we wrapped the mandrel and conductor with an adhesive glass cloth electrical tape (3M Scotch® 27) to help constrain the turns (figure 4). The magnets were not impregnated due to the low electromagnetic

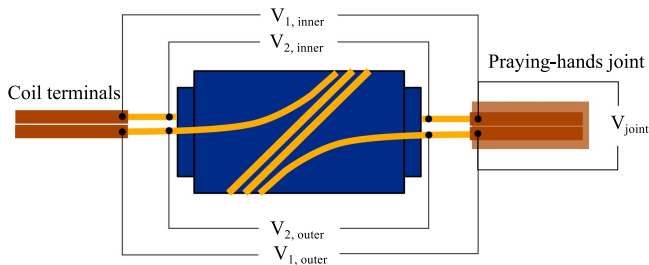


**Figure 5.** Voltage tap configuration for magnets C0a and C0b. Each layer had two pairs of voltage taps:  $V_1$  pair terminated inside the Cu terminals and  $V_2$  pair was soldered to the wires next to the mandrels.

forces expected during the test (less than 20 N per mm in the peak field region of the magnet).

To assemble both layers into the dipole magnet configuration, the inner layer was first inserted into the outer layer. They were then anchored to a G10 support board using Brass screws through the alignment holes on the mandrels which also aligned the layers axially (figure 3). We inserted G10 shims into the radial gap between the layers to center the inner layer. An assembly of a cryogenic Hall sensor (Lakeshore HGCT 3020) was then anchored to the Brass screws to position the Hall sensor within 1 mm to the center of magnet aperture (figure 4).

Electrical joints were made using the Cu terminals at wire ends. These hollow Cu terminals were 150–200 mm long with an outer diameter (OD) of 6.35 mm. They were soldered to the CORC® wires by ACT using Sn63Pb37 for magnet C0a and indium solder for magnet C0b.

At lead end, we sandwiched the Cu terminal into a pair of Cu blocks with grooves matching the OD of the Cu terminals and indium foils. The Cu blocks were then pressed against each other by screws to create a pressure contact between the wire terminals and Cu blocks. At return end, the terminals from both layers were sandwiched into a pair of Cu blocks to form a praying-hands joint (figure 4). NbTi Rutherford cables connected the Cu blocks to vapor-cooled current leads of the test stand.

#### 4. Experimental setup and test protocol

Several voltage taps were installed to measure the voltage evolution during the current ramp. The first pair of voltage taps ( $V_1$ ) was installed inside the Cu terminal (figure 5). The second pair ( $V_2$ ) was soldered to the CORC® wire after the magnet was assembled. The  $V_2$  taps were each about 3 mm away from the end of mandrel to reduce the resistive voltage due to the current transfer inside the Cu terminal. The  $V_2$  voltage tap wires were wrapped and soldered around the CORC® wire, in direct contact with the outer most layer of tapes. The  $V_2$  wires for magnet C0b were co-wound with CORC® wire to reduce inductive noise during current ramp. The resistance of the return-end joints was measured with the two voltage taps inside the Cu terminal (figure 5).

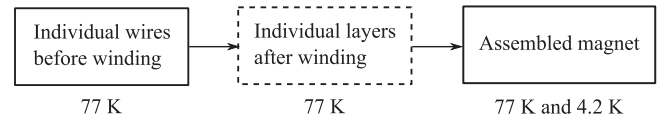


**Figure 6.** Test protocol of CORC® wires and magnets.

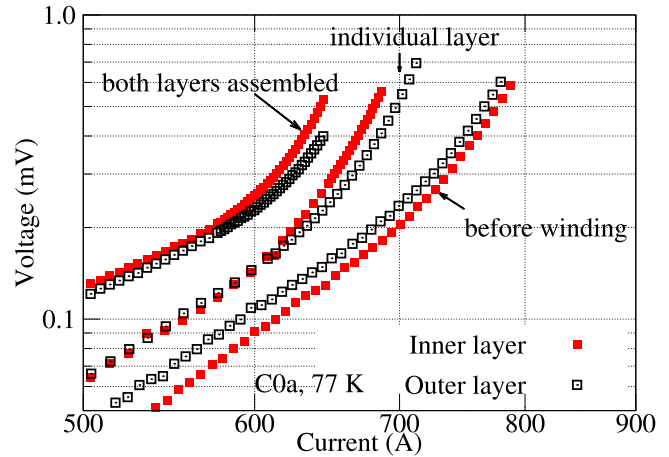


**Figure 7.** Wire voltage as a function of current for magnet C0a: before winding, the individual layer after winding, and each layer after being assembled into the CCT dipole configuration. 77 K, self-field, log–log scale.

Signals from the voltage taps and Hall sensor were measured with digital multimeters (Tektronix 2182A) via a GPIB bus. The typical measurement rate was 0.5–1 Hz.

To evaluate the impact of coil winding on the transport performance of CORC® wires, we measured the voltage across wires as a function of current at two stages of assemble (figure 6): before winding at 77 K and after assembly into CCT dipole magnets at 77 and 4.2 K. Each layer of magnet C0a was also tested separately at 77 K.

The 77 K tests of the wires and magnets used a stair-step current profile with a 2 kA power supply to minimize the inductive pickup. For the 4.2 K test, a 25 kA power supply was used. Current ramped continuously and reduced to zero when the peak layer voltage was less than 1 mV. The  $V_2$  voltage taps were used for the 4.2 K tests.

C0a had three tests at 77 K followed by four tests at 4.2 K and one last test at 77 K. C0b had four tests at 77 K followed by one test at 4.2 K. Both magnets were cooled down from room temperature for each test. Two Lakeshore Cernox thermometers, one on each end of magnet mandrels, monitored the temperature profiles during cooldown. The maximum cooldown rate was 50 K h<sup>−1</sup>.

#### 5. Test results

##### 5.1. Current-carrying capability of the 16-tape wire and CCT magnet C0a at 77 K, self-field

Figure 7 compares the voltage versus current at 77 K for the 16-tape CORC® wires during the fabrication of magnet C0a.



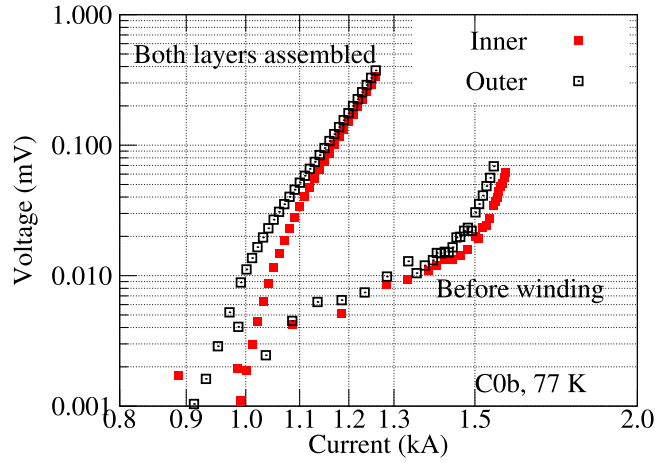


**Figure 8.** Wire voltage as a function of current for magnet C0b: before winding and after being assembled into the CCT dipole magnet. 77 K, self-field, log–log scale.

**Table 3.** Wire  $I_c$  for magnet C0a at different stages, 77 K and self-field.  $E_c = 1 \mu\text{V cm}^{-1}$ .

	Inner layer wire (160711-056A)		Outer layer wire (160711-056B)	
	$I_c$ (A)	$n$	$I_c$ (A)	$n$
Before winding	754	8.7	741	7.6
Each layer tested individually after winding	672	13.5	685	12.6
Each layer in the CCT dipole configuration	645	14	663	8

**Table 4.** Wire  $I_c$  for magnet C0b at 77 K and self-field.  $E_c = 1 \mu\text{V cm}^{-1}$ . The  $I_c$  and  $n$  values were determined up to the measured peak voltages as shown in figure 8.

	Inner layer wire (170131-1)		Outer layer wire (170131-2)	
	$I_c$ (A)	$n$	$I_c$ (A)	$n$
Before winding	1675	31.6	1644	28.8
Each layer in the CCT dipole configuration	1247	16.4	1239	15

Table 3 compares  $I_c$  and  $n$  value determined with an electric-field criterion of  $1 \mu\text{V cm}^{-1}$  up to the measured peak voltage (figure 7). After winding, the  $I_c$  of the inner layer decreased by 11% and the  $I_c$  of the outer layer decreased less by 8%. The  $I_c$  of both layers decreased by another 4% after the assembly into the dipole magnet configuration.

## 5.2. Current-carrying capability of the 29-tape wire and CCT magnet C0b at 77 K, self-field

Figure 8 compares the voltage of each layer before winding and after being assembled into magnet C0b.

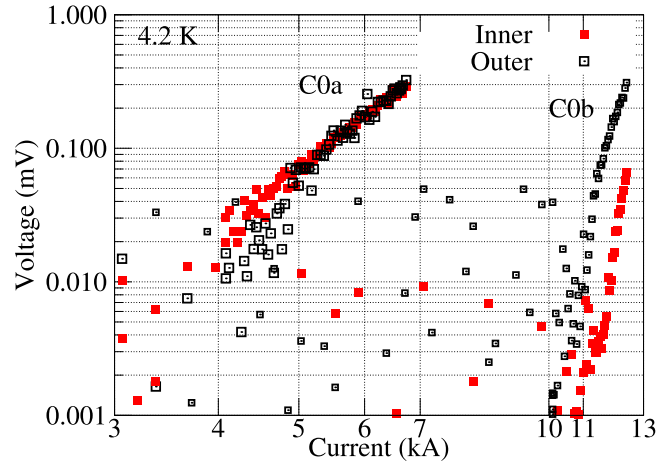


**Figure 9.** Layer voltage as a function of current for both magnets at 4.2 K, self-field, log–log scale.

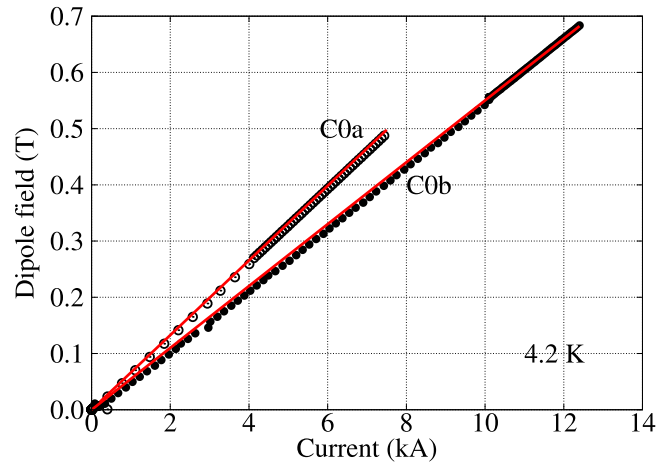


**Figure 10.** Dipole fields at the center of magnet aperture. Points: measurement. Lines: calculation.

$I_c$  of both wires decreased by 25% at 77 K after being wound and assembled into the dipole configuration (table 4). The  $n$  values of both layers decreased by 50% after winding.

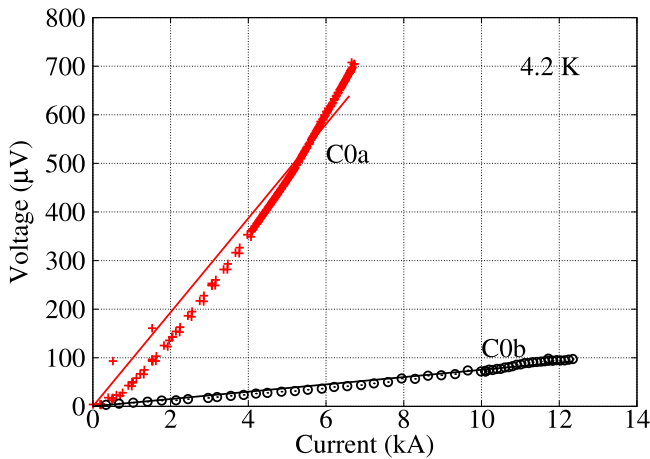
## 5.3. Current-carrying capability of both magnets at 4.2 K, self-field

Figure 9 compares the layer voltage of both magnets during the current ramp at 4.2 K, self-field. The peak current was 6748 A for C0a ( $J_c = 900 \text{ A mm}^{-2}$ ) and 12 402 A for C0b ( $J_c = 1198 \text{ A mm}^{-2}$ ), about a factor of 10 increase from 77 K.

C0a started to exhibit a detectable voltage rise at 4.1 kA, 72% of the expected short-sample limit. For C0b, the outer layer started the transition at 11 kA, 87% of the short-sample limit, followed by the inner layer at 11.8 kA. More details on the short-sample limit can be found in the [appendix](#).

## 5.4. Dipole field at the center of magnet aperture

Figure 10 compares the measured and calculated dipole fields at the center of magnet aperture. The calculation was based on the Biot–Savart law and considered actual wire location



**Figure 11.** The voltage across the return-end joint as a function of current at 4.2 K.

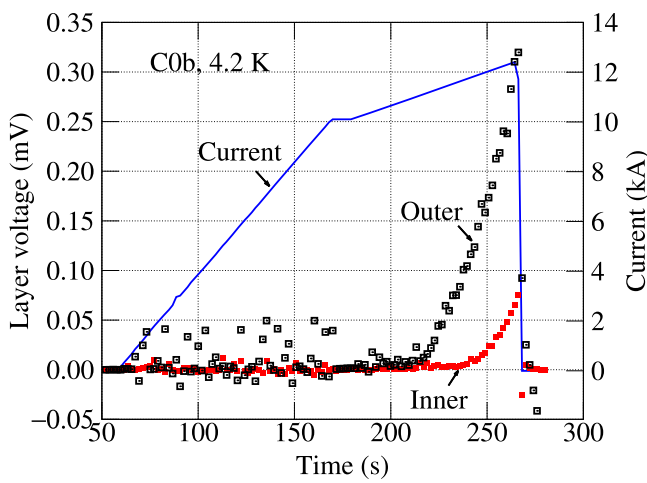


**Figure 12.** The layer voltage and current of C0b as a function of time at 4.2 K, self-field. The outer layer conductor burned out at the peak current of 12.4 kA.

including both ends as shown in figure 3. The difference between the measurements and calculation was within 1.3% for C0a and 0.4% for C0b. The discrepancy was consistent with the 1 mm tolerance of the Hall probe center with respect to the magnet center. Magnet C0a had a transfer function of  $66.4 \mu\text{T A}^{-1}$ , 19% higher than that of C0b ( $55.6 \mu\text{T A}^{-1}$ ).

### 5.5. Joint resistance

Figure 11 shows the voltage as a function of current at 4.2 K for both magnets. The joint resistance also included the contribution from the Cu blocks of the joint structures and contact resistance from the indium foils. A linear fit of the measured voltages gives a resistance of  $97 \text{ n}\Omega$  in C0a and  $8 \text{ n}\Omega$  in C0b.

### 5.6. Wire burn-out due to over-heating

C0b outer layer developed a hot spot that damaged the wire at 12.4 kA during the 4.2 K test when the layer voltages developed to a similar level at 77 K (figure 12). The voltage

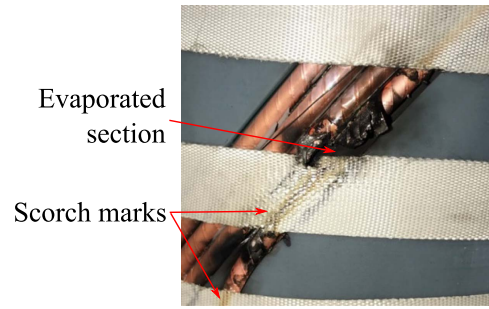


**Figure 13.** Wire burned out at the peak field region in the outer layer of C0b.

across the outer layer started rising at 11 kA ( $J_e \sim 1000 \text{ A mm}^{-2}$ ) and the resistive heating continued for about 50 s until the wire burned out at 12.4 kA ( $J_e \sim 1200 \text{ A mm}^{-2}$ ).

The wire burned out at the peak field region in the outer layer (figure 13). A wire section, about 5 mm in length, evaporated at the burnt location. The growing normal zone also melted the polyester heat shrink tube and scorched the white tape that crossed over the wires (figure 13). The melted shrink tube and scorch marks covered about 200 mm length along the wire.

## 6. Discussion

### 6.1. CCT dipole magnets using REBCO CORC® wires is a viable technology

The scalability of the CCT design allowed us to effectively develop and demonstrate fundamental magnet technology features such as magnet design, winding, joints and testing with relatively short conductor lengths. The test results clearly showed that the concept of CCT magnets using the CORC® round wires is viable. We can make larger magnets featuring more turns, higher fields and increased stored energies that will be well suited to study conductor stress, field quality, quench protection and their behavior in high background fields.

The prototype CORC® wires used here were robust for the react-and-wind magnet fabrication approach. After magnet fabrication, the 16-tape wire retained at least 85% of the critical current measured before winding at 77 K self-field, with at least 4% out of the 15% reduction due to an increased field on the wire after winding and both layers were assembled. The 29-tape wire retained at least 75% of the critical current measured at 77 K self-field before winding. The higher current reduction in C0b at 77 K was likely caused by higher fields on the wire in C0b at 1.2 kA (163 mT) as opposed to 650 A for C0a (101 mT). The critical current of a solenoid magnet wound with round REBCO cables shows a similar strong sensitivity to the magnetic field at 77 K [38]. In addition, the wires showed no  $I_c$  degradation after thermal cycles between room temperature and 77/4.2 K with a maximum cooldown rate of  $50 \text{ K h}^{-1}$ .

At 4.2 K, both magnets showed a resistive voltage at a current lower than the expectation: magnet C0a at 72% of the

short-sample limit and magnet C0b at 87% of the short-sample limit. One explanation is that the magnet fabrication and/or the cold test may have degraded the conductors. But the uncertainty of the estimated  $I_c(B)$  data at low field can also over estimate the expected short-sample limit (appendix). This suggests a strong need to measure the wire  $I_c(B)$  and its uniformity along the entire wire length that can provide reliable prediction of magnet performance.

The CCT dipole magnets using CORC<sup>®</sup> wires were relatively simple to fabricate. A mandrel with grooves cut into it to place the wires was enough to wind the CCT magnets as opposed to multiple end parts that are used for a REBCO  $\cos \theta$  dipole magnet design [20]. The fact that the REBCO wires do not require a heat treatment after winding allows more options for mandrel material and manufacturing. For instance, the mandrels for magnets C0a and C0b were 3D printed, further simplifying the fabrication for the three-turn dipole magnets.

The groove design reported here can allow continuous and automated winding that will be required for magnets with more turns. With this design, CCT dipole magnets can be wound similar to solenoids, greatly reducing wire handling that would otherwise be required during magnet winding and potential risk of wire damage. Recently we developed a prototype winding setup and successfully wound 40 turns of CORC<sup>®</sup> wire on a 0.5 m long mandrel. More details will be reported elsewhere.

The wire terminal based on the tapered layers of tapes and a Cu tube [39, 40] enabled straightforward joint development between CCT coils and between magnets and current buss bars. With indium solder inside the Cu terminals, we achieved an 8 n $\Omega$  resistance between two CORC<sup>®</sup> wires through their Cu terminals with pressure contacts and indium foils. Soldering CORC<sup>®</sup> wires inside a Cu terminal, instead of pressure contact, can further reduce the joint resistance.

Further development of CCT dipole magnets will provide effective input to optimize REBCO tapes and CORC<sup>®</sup> wires based on magnet performance. This in turn can further improve magnet performance. Developing CORC<sup>®</sup> CCT magnets will also allow to compare with the performance and cost of other high-temperature superconducting accelerator magnet concepts and prototypes, which will be critical for future high-field accelerator magnet applications.

Although the CORC<sup>®</sup> CCT concept offers a viable technology option for REBCO accelerator magnets, several further developments are required to achieve high-field CCT magnets. They are discussed in the following sections.

## 6.2. Increasing $J_e$ and reducing minimum allowable bending radius of CORC<sup>®</sup> wires

REBCO accelerator insert magnets need to generate high magnetic fields in a compact form to fit into the limited aperture of outsert magnets. For CCT designs, this requirement calls for magnet conductors with a high  $J_e$  at a small bending radius.

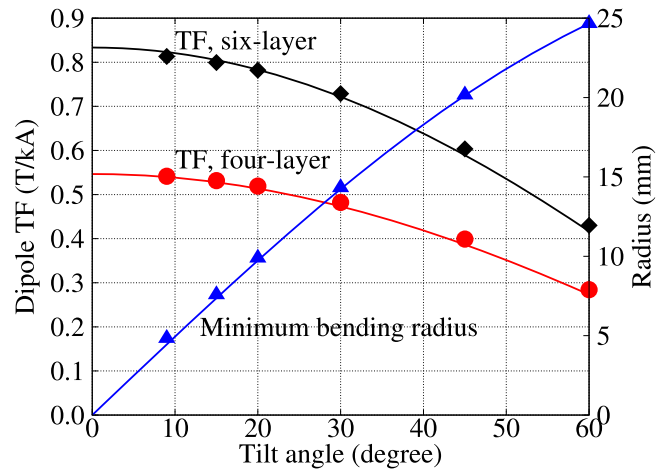


**Figure 14.** Dipole transfer function (TF) and minimum bending radius as a function of the tilt angle for two multi-layer CCT dipole magnets. Each layer has 40 turns of wires. The magnet aperture is 50 mm.

As an example, the dipole transfer function of C0b is 16% lower than that of C0a (figure 10), even though C0b carried almost twice the current of C0a. This is because the 29-tape wire used in C0b was bent to a radius of 30 mm to avoid significant current degradation. It was 20% larger than the 25 mm bending radius for the 16-tape wire used in C0a. Therefore, with the same tilt angle, the mandrel for C0b had a larger diameter (table 2) which lead to a lower transfer function.

Let us consider two multi-layer CCT dipole magnet designs based on the experience of C0a and C0b to gain some insight into the requirements for CORC<sup>®</sup> wires. Both designs have a magnet aperture of 50 mm. The first design has four layers with an OD of 97 mm. The second design has six layers with an OD of 121 mm. For both designs, each layer has 40 turns of wires with a wire diameter of 3.7 mm (similar to the 29-tape wire). All the layers in each design have the same tilt angle. The radial gap between the layers is 0.5 mm and the rib thickness at the mid-plane is also 0.5 mm (table 2).

Figure 14 plots the dipole transfer function and minimum bending radius as a function of the tilt angle  $\alpha$ . The transfer function is proportional to  $\cos \alpha$  and the minimum bending radius is proportional to  $\sin \alpha$  [29, 33, 41].

With a tilt angle of 30°, the four-layer design has a transfer function of 0.48 T kA<sup>-1</sup> and a minimum bending radius of 15 mm. The wire needs to carry 10.4 kA to generate 5 T dipole fields in a background field of 16 T at 4.2 K. This leads to a wire  $J_e$  of 960 A mm<sup>-2</sup> at 21 T, 4.2 K and 15 mm bending radius, assuming the peak field on CORC<sup>®</sup> wire is similar to that in the aperture. The wire  $J_e$  can be further reduced to 830 A mm<sup>-2</sup> at 21 T if we implement the following two changes: (1) reduce the tilt angle for layer 3 and 4 such that wires in layer 1 and 3 have the same 15 mm bending radius, and (2) reduce the thickness of the mid-plane ribs to zero.

At the same 30° tilt angle, the six-layer CCT dipole design has a transfer function of 0.73 T kA<sup>-1</sup>, 51% higher than that of the four-layer design (figure 14). The wire needs

**Table 5.** Minimum wire  $J_c$  for two CCT dipole insert magnet designs to generate 5 T in a background field of 16 T at 4.2 K. The  $J_c$  is for a CORC<sup>®</sup> wire with a diameter of 3.7 mm at a bending radius of 15 mm. The values at 16 T are determined assuming a power-law field dependence of  $J_c \propto B^{-0.9}$  [44].

Number of layers	ID mm	OD mm	21 T A mm <sup>-2</sup>	16 T A mm <sup>-2</sup>
4	50	97	830	1060
6	50	121	540	690

to carry 6.9 kA to generate 5 T in a background field of 16 T at 4.2 K. This corresponds to a wire  $J_c$  of 640 A mm<sup>-2</sup> at 21 T, 4.2 K and 15 mm bending radius. It can be further reduced to 540 A mm<sup>-2</sup> at 21 T if we implement similar optimization mentioned above.

For a no-iron, perfect  $\cos \theta$  current distribution, the dipole field is proportional to the coil width [42, 43]. The 1.5 ratio between the dipole transfer functions of two designs (figure 14) agrees with this analytic result because here the coil width is proportional to the number of layers.

Table 5 summarizes the minimum  $J_c$  for two designs to generate 5 T dipole fields in the background field of 16 T. For comparison, the 16-tape wire used in C0a is expected to have a  $J_c$  of about 120 A mm<sup>-2</sup> at 21 T, 4.2 K and 25 mm bending radius. The 29-tape wire used in C0b is expected to have a  $J_c$  of 220 A mm<sup>-2</sup> at 21 T, 4.2 K and 30 mm bending radius.

Thinner REBCO tapes with higher  $J_c$  will be critical to reach a minimum 540 A mm<sup>-2</sup> wire  $J_c$  at 21 T, 4.2 K and 15 mm bending radius. The wires reported here were enabled by REBCO tapes with 30  $\mu$ m thick substrates from SPI [26]. With thinner substrates, one can use thinner formers in the CORC<sup>®</sup> wire, which can increase  $J_c$  and improve the flexibility of CORC<sup>®</sup> wire to potentially allow bending to below 15 mm radius. SPI is developing tapes with 25  $\mu$ m thick substrates. They are expected to become a standard product within the next 12–24 months. Increasing the fill factor with thicker REBCO layer can also be effective to achieve a higher  $J_c$ , as recently demonstrated by Xu *et al* with a 3.2  $\mu$ m thick REBCO layer that reaches a  $J_c$  of 2000 A mm<sup>-2</sup> at 4.2 K, 16 T [44].

### 6.3. Detecting normal zones soon enough to prevent conductor burn-out

Due to the rapid temperature rise in the normal zone, the criteria for magnet quench protection should be derived from the allowable hot-spot temperature. The large Cu current density ( $J_{Cu}$ ) in the normal zone, together with the slow quench propagation, can result in burn-out if the resistive voltage is allowed to rise too high. This is because the hot-spot temperature increases with  $J_{Cu}^2$  and the heating time since the normal zone initiates [45, 46]. The current of C0b increased by a factor of 10 from 77 to 4.2 K, leading to a  $J_c$  above 1000 A mm<sup>-2</sup> and a  $J_{Cu}$  of more than 2000 A mm<sup>-2</sup> in

the wire section that turned normal (table 1). The high  $J_{Cu}$  of C0b at 4.2 K clearly contributed to the burn-out when the layer voltage approached to the same level at 77 K.

The evaporated wire section in C0b (figure 13) indicated that the peak temperature of the normal zone was over 1356 K, the melting temperature of Cu. To limit the peak temperature on a single REBCO tape to below 200 K, one needs to detect the quench and start energy extraction within 50 ms with a  $J_{Cu}$  of 2000 A mm<sup>-2</sup> in an adiabatic condition [47]. Thus, it is essential to detect normal zones early.

Although figure 12 shows that detecting quench with resistive voltage signals was clearly feasible for C0b with a  $J_c$  of 1000 A mm<sup>-2</sup> that is above the target for future CORC<sup>®</sup> CCT magnets, other techniques such as the fiber-optic [48] and acoustic thermometry [49] should be evaluated for early detection of magnet quenches. These new techniques can be indispensable when the voltage taps are either unavailable or ineffective due to the strong electromagnetic background noises.

The discussion here implies that current can share between REBCO tapes and between the tapes and Cu former for a CORC<sup>®</sup> wire. Without sufficient current sharing,  $J_{Cu}$  would be higher and further challenge the quench detection. Understanding current sharing in CORC<sup>®</sup> wires will be an important next step.

As a side note in section 5.3 we characterized the 4.2 K magnet performance with the current at which the layer voltage rose to a level that can be detected by a quench detection scheme. In our opinion, a critical current based on an electric-field criterion will not be suitable for future CORC<sup>®</sup> REBCO magnets. First, the critical current would depend on the conductor length. Second, it can risk damaging magnets at 4.2 K for the reasons discussed earlier.

### 6.4. Other critical needs for high-field CCT magnets using CORC<sup>®</sup> wires

The REBCO conductors will experience strong Lorentz forces when operating in high background fields. Conductor degradation due to Lorentz forces has been observed in REBCO high-field solenoid insert coils [50, 51] and high-current fusion cables [52, 53]. In addition, the groove design reported here can only partially support the wire against the Lorentz force at the pole region of the CCT dipole magnets.

A mechanism such as epoxy impregnation [4, 5, 54, 55] is needed to support the wire and to prevent it from moving. Metal mandrels with high strength and possible manufacturing routes other than machining should be investigated.

As discussed earlier, accurate measurements of the transport performance of CORC<sup>®</sup> wires as a function of magnetic fields are required to determine the expected magnet performance and assess the magnet fabrication technology. The measurements should be performed at the bending radii relevant for magnet developments.



## 7. Conclusion

We have successfully demonstrated the CCT dipole magnet concept through the design, fabrication and testing of two double-layer three-turn CCT dipole magnets using CORC<sup>®</sup> wires. Magnet C0a was wound with a 16-tape wire and magnet C0b used a 29-tape wire. Both wires used 2 mm wide tapes with 30  $\mu\text{m}$  thick substrate produced by SPI. At least 75% of the current-carrying capability of the CORC<sup>®</sup> wires was retained after being wound into CCT magnets based on the measurements at 77 K, self-field. The magnets generated dipole fields ranging from 0.5 to 0.7 T, consistent with the calculation based on the Biot–Savart law. CCT dipole magnets using CORC<sup>®</sup> wires is a viable option for future high-field accelerator insert magnets using REBCO conductors.

To generate a 5 T dipole field with a four-layer CCT insert magnet with 50 mm aperture and 100 mm OD in a 16 T background field, a minimum wire  $J_c$  of 830 A mm<sup>-2</sup> would be required in a 3.7 mm diameter CORC<sup>®</sup> wire at a bending radius of 15 mm and 21 T, 4.2 K. The required  $J_c$  reduces to 540 A mm<sup>-2</sup> when the same CORC<sup>®</sup> wire is used to wind a six-layer CCT magnet with an OD of 121 mm. Sensitive quench detection and sufficient current sharing inside the wire are needed to protect future magnets using CORC<sup>®</sup> wires with such a high  $J_c$  from quench-induced degradation. The three-turn magnet platform demonstrated here allows us to effectively progress toward these targets with minimum resources.

We intend to develop and demonstrate CORC<sup>®</sup> CCT dipole magnets with more turns and higher fields as part of the next steps. Building magnets and understanding their behaviors will help to further optimize the performance of REBCO tapes and wires to achieve the desired magnet performance.

## Acknowledgments

We thank Arno Godeke (now with Varian Medical Systems Particle Therapy GmbH) who initiated the study of CCT magnets using CORC<sup>®</sup> conductors. We also thank Diego Arbelaez, Lucas Brouwer, Ray Hafalia, Thomas Lipton, Maxim Marchevsky, Emmanuele Ravaioli, Tengming Shen, Jordan Taylor, Marcos Turquiti and Liyang Ye (now with GE Healthcare) for discussions and help during the coil development and test. The work is supported by the US Department of Energy under contracts DE-SC0009545, DE-SC0014009, and DE-SC0015775. The work at LBNL was also supported by the Director, Office of Science, Office of High Energy Physics, and Office of Fusion Energy Sciences, of the US Department of Energy under Contract No. DE-AC02-05CH11231.

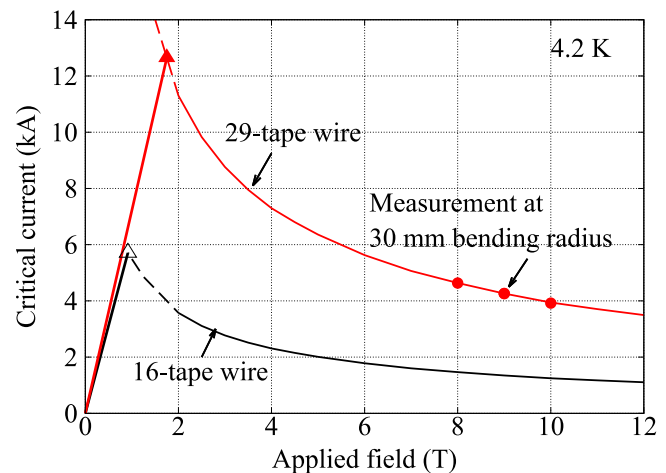


**Figure A1.** The  $I_c$  at 4.2 K as a function of applied magnetic field for a 16-tape wire bent to a 25 mm radius (black line) and a 29-tape wire bent to a 30 mm radius (red line) linearly scaled from the data of the 16-tape wire. The round solid points are measured data from [56]. The straight lines are the load lines on the wires for each magnet. The triangles are the expected short-sample limits.

## Appendix. The expected magnet performance (short-sample limit)

The expected magnet performance is determined based on the conductor  $I_c(B)$  data and the peak field on the conductor that is normal to the conductor surface. Figure A1 plots the  $I_c$  of the 16-tape and 29-tape CORC<sup>®</sup> wires as a function of applied magnetic fields at 4.2 K. The self-field contribution was neglected to simplify the analysis.

The  $I_c$  of the 16-tape wire was estimated based on the transport performance of one single sample tape. The  $I_c$  of the sample tape was measured typically from 15 to 2 T at the Applied Superconductivity Center, National High Magnetic Field Laboratory. The  $I_c$  below 2 T was extrapolated from the values at higher fields (dashed lines in figure A1).

The  $I_c$  of the 29-tape wire was measured at University of Twente at 8, 9 and 10 T applied fields, 4.2 K [56]. The wire was bent on a sample holder with a radius of 30 mm, similar to the minimum bending radius of the wire used in C0b. The  $I_c(B)$  for the 29-tape wire was obtained by linearly scaling the  $I_c(B)$  data of the 16-tape wire and matching the data for the 29-tape wire measured at 8, 9 and 10 T.

With the load lines of both magnets (straight lines in figure A1), we determined that the short-sample limit at 4.2 K is 5707 A for C0a and 12645 A for C0b.

## ORCID iDs

Xiaorong Wang <https://orcid.org/0000-0001-7065-8615>  
Danko van der Laan <https://orcid.org/0000-0001-5889-3751>

## References

- [1] Tommasini D et al 2017 *IEEE Trans. Appl. Supercond.* **27** 4000405
- [2] Xu Q et al 2016 *IEEE Trans. Appl. Supercond.* **26** 4000404
- [3] Matias V and Hammond R H 2012 *Phys. Proc.* **36** 1440–4
- [4] Trociewitz U P, Dalban-Canassy M, Hannion M, Hilton D K, Jaroszynski J, Noyes P, Viouchkov Y, Weijers H W and Larbalestier D C 2011 *Appl. Phys. Lett.* **99** 202506
- [5] Maeda H and Yanagisawa Y 2014 *IEEE Trans. Appl. Supercond.* **24** 4602412
- [6] Senatore C, Alessandrini M, Lucarelli A, Tediosi R, Uglietti D and Iwasa Y 2014 *Supercond. Sci. Technol.* **27** 103001
- [7] Weijers H W et al 2016 *IEEE Trans. Appl. Supercond.* **26** 4300807
- [8] Yoon S, Kim J, Cheon K, Lee H, Hahn S and Moon S H 2016 *Supercond. Sci. Technol.* **29** 04LT04
- [9] Hahn S 2017 Mini magnet packs world-record, one-two punch <https://nationalmaglab.org/news-events/news/mini-magnet-packs-world-record-punch>
- [10] Zangenberg N, Nielsen G, Hauge N, Nielsen B, Baurichter A, Pedersen C, Brauner L, Ulsoe B and Moller S 2012 *IEEE Trans. Appl. Supercond.* **22** 4004004
- [11] Amemiya N et al 2015 *IEEE Trans. Appl. Supercond.* **25** 4003505
- [12] Koyanagi K, Takayama S, Miyazaki H, Tosaka T, Tasaki K, Kurusu T and Ishii Y 2015 *IEEE Trans. Appl. Supercond.* **25** 4003104
- [13] Bogdanov I V et al 2016 *Supercond. Sci. Technol.* **29** 105012
- [14] Gupta R et al 2015 *IEEE Trans. Appl. Supercond.* **25** 4003704
- [15] Bottura L and Godeke A 2012 *Rev. Accel. Sci. Technol.* **5** 25–50
- [16] Rossi L et al 2015 *IEEE Trans. Appl. Supercond.* **25** 4001007
- [17] Kirby G et al 2015 *IEEE Trans. Appl. Supercond.* **25** 4000805
- [18] Goldacker W, Grilli F, Pardo E, Kario A, Schlachter S I and Vojenčiak M 2014 *Supercond. Sci. Technol.* **27** 093001
- [19] van Nugteren J, Kirby G, de Rijk G, Rossi L, ten Kate H and Dhalle M 2015 *IEEE Trans. Appl. Supercond.* **25** 4000705
- [20] Lorin C, Durante M, Fazilleau P, Kirby G and Rossi L 2016 *IEEE Trans. Appl. Supercond.* **26** 4003105
- [21] van Nugteren J et al 2018 *Supercond. Sci. Technol.* submitted
- [22] Takayasu M, Chiesa L, Bromberg L and Minervini J V 2012 *Supercond. Sci. Technol.* **25** 014011
- [23] Himbele J J, Badel A and Tixador P 2016 *IEEE Trans. Appl. Supercond.* **26** 4005205
- [24] van der Laan D C, Lu X F and Goodrich L F 2011 *Supercond. Sci. Technol.* **24** 042001
- [25] van der Laan D C, Weiss J D, Noyes P, Trociewitz U P, Godeke A, Abraimov D and Larbalestier D C 2016 *Supercond. Sci. Technol.* **29** 055009
- [26] Weiss J D, Mulder T, ten Kate H J and van der Laan D C 2017 *Supercond. Sci. Technol.* **30** 014002
- [27] Vojenčiak M, Kario A, Ringsdorf B, Nast R, van der Laan D C, Scheiter J, Jung A, Runtsch B, Gömöry F and Goldacker W 2015 *Supercond. Sci. Technol.* **28** 104006
- [28] Meyer D and Flasck R 1970 *Nucl. Instrum. Methods* **80** 339–41
- [29] Goodzeit C L, Ball M J and Meinke R B 2003 *IEEE Trans. Appl. Supercond.* **13** 1365–8
- [30] Gavrilin A V, Bird M D, Bole S T and Eyssa Y M 2002 *IEEE Trans. Appl. Supercond.* **12** 465–9
- [31] Devred A et al 2006 *Supercond. Sci. Technol.* **19** S67
- [32] Caspi S et al 2014 *IEEE Trans. Appl. Supercond.* **24** 4001804 and references therein
- [33] Brouwer L N 2015 Canted-cosine-theta superconducting accelerator magnets for high energy physics and ion beam cancer therapy *PhD Thesis* University of California, Berkeley <https://escholarship.org/uc/item/8jp4g75g>
- [34] Caspi S, Arbelaez D, Brouwer L, Gourlay S, Prestemon S and Auchmann B 2017 *IEEE Trans. Appl. Supercond.* **27** 4001505
- [35] Godeke A et al 2015 *IEEE Trans. Appl. Supercond.* **25** 4002404
- [36] 3D Systems <https://3dsystems.com/materials/accura-bluestone>
- [37] Fessia P 2013 The new 3D printing facility at the CERN polymer lab <https://indico.cern.ch/event/271447/>
- [38] Šouc J, Gömöry F, Vojenčiak M, Seiler E, Kováč J and Frolek L 2017 *Supercond. Sci. Technol.* **30** 105014
- [39] Mulder T, Dudarev A, van der Laan D C, Mentink M G T, Dhallé M and ten Kate H H J 2015 Optimized and practical electrical joints for CORC type HTS cables *IOP Conf. Ser.: Mater. Sci. Eng.* **102** 012026
- [40] van der Laan D 2017 Superconducting cable connections and methods *US Patent* 9,755,329
- [41] Wang X, Arbelaez D, Caspi S, Prestemon S O, Sabbi G and Shen T 2017 *IEEE Trans. Appl. Supercond.* **27** 6604010
- [42] Caspi S and Ferracin P 2005 Limits of Nb<sub>3</sub>Sn accelerator magnets *Proc. of 2005 Particle Accelerator Conf.* pp 107–11
- [43] Rossi L and Bottura L 2012 *Rev. Accel. Sci. Technol.* **5** 51–89
- [44] Xu A et al 2017 *Sci. Rep.* **7** 6853
- [45] Wilson M N 1983 *Superconducting Magnets* (New York: Oxford University Press) ch 9
- [46] Iwasa Y 2009 *Case Studies in Superconducting Magnets: Design and Operational Issues* 2nd edn (Berlin: Springer) ch 8
- [47] Wang X, Trociewitz U P and Schwartz J 2011 *Supercond. Sci. Technol.* **24** 035006
- [48] Scurti F, Ishmael S, Flanagan G and Schwartz J 2016 *Supercond. Sci. Technol.* **29** 03LT01
- [49] Marchevsky M and Gourlay S A 2017 *Appl. Phys. Lett.* **110** 012601
- [50] Kajita K et al 2016 *IEEE Trans. Appl. Supercond.* **26** 4301106
- [51] Kajita K, Takao T, Maeda H and Yanagisawa Y 2017 *Supercond. Sci. Technol.* **30** 074002
- [52] Uglietti D, Bykovsky N, Sedlak K, Stepanov B, Wesche R and Bruzzone P 2015 *Supercond. Sci. Technol.* **28** 124005
- [53] Bykovsky N, Uglietti D, Sedlak K, Stepanov B, Wesche R and Bruzzone P 2016 *Supercond. Sci. Technol.* **29** 084002
- [54] Michael P C, Haight A E, Bromberg L and Kano K 2015 *IOP Conf. Ser.: Mater. Sci. Eng.* **102** 012019
- [55] Otten S, Kario A, Kling A and Goldacker W 2016 *Supercond. Sci. Technol.* **29** 125003
- [56] Mulder T, Weiss J, van der Laan D, Dhallé M and ten Kate H 2018 Development of ReBCO-CORC wires with current densities of 400 to 600 A mm<sup>-2</sup> at 10 T and 4.2 K *IEEE Trans. Appl. Supercond.* **28** 4800504